ADVANCED SCIENCE Open Access
www.advancedscience.com

Recent Developments and Future Perspectives of Molybdenum Borides and MBenes

Chandra Sekhar Rout, Pratik V. Shinde, Abhinandan Patra, and Sang Mun Jeong**

Metal borides have received a lot of attention recently as a potentially useful material for a wide range of applications. In particular, molybdenum-based borides and MBenes are of great significance, due to their remarkable properties like good electronic conductivity, considerable stability, high surface area, and environmental harmlessness. Therefore, in this article, the progress made in molybdenum-based borides and MBenes in recent years is reviewed. The first step in understanding these materials is to begin with an overview of their structural and electronic properties. Then synthetic technologies for the production of molybdenum borides, such as high-temperature/pressure methods, physical vapor deposition (PVD), chemical vapor deposition (CVD), element reaction route, molten salt-assisted, and selective etching methods are surveyed. Then, the critical performance of these materials in numerous applications like energy storage, catalysis, biosensors, biomedical devices, surface-enhanced Raman spectroscopy (SERS), and tribology and lubrication are summarized. The review concludes with an analysis of the current progress of these materials and provides perspectives for future research. Overall, this review will offer an insightful reference for the understanding molybdenum-based borides and their development in the future.

1. Introduction

Recently, transition metal borides (TMBs) have gained renowned interest due to their remarkable diversity in structure and topology leading to unique tunable physical and chemical properties.[1–3] Most of the TMBs share M—B bonds with the strong covalent component and these bonds are stronger than those in the case of transition metal nitrides and carbides.[4] Further, due to the existence of strong and highly covalent B—B bonds, TMBs exhibit numerous compositions ranging from M_3B to MB_{66} with varying characteristics from metallic to semiconducting states. Due to their diverse compositions and crystal structures, TMBs have a wide range of interesting electronic ground states, thus featuring high chemical, mechanical, magnetic, and catalytic characteristics, thermal durability, thermoelectricity, structural complexity, and superconductivity.[5,6] Therefore, as compared to other non-metal atoms (e.g., S, O, N) in the corresponding compounds of sulfides, oxides, and nitrides, boron atoms in metal borides have several superior properties due to the chemical nature of boron.[3] Boron is a metalloid element with an intermediate electronegativity (2.04 in the Pauling scale) between metals and non-metals. Due to this reason, a large variety of bond types in borides such as metallic bonds M—M/M—B, ionic bond M—B, and covalent bonds B—B are possible.[7] Boron becomes electron deficient because there is less number of valence electrons available than valence orbitals, allowing it for a wide variety of linking patterns in boride lattices.[8] In addition, compared to the phosphorization and sulfurization processes, boride synthesis produces significantly lower harmful gases and is, therefore, more environmentally friendly. Therefore, TMBs offer excellent potential for growing areas of research and many discoveries due to unique boron chemistry and the possibility of making the diversity of boride composition and structure. 2D transition metal borides, abbreviated MBenes, are produced by selectively etching the A layer from multi-layered structure (MAB phases).[9–11] The M—A bond is metallic, whereas the M—B bond exhibits mixed covalent/metal/ionic characteristics. The difference between MBenes and MXenes appears to be the substitution of boron in the carbon and/or nitrogen sites of MXenes. However, because of variations in the stoichiometry and structural transitions, the MAB-MBenes cannot be directly linked to the MAX-MXenes combination. MBenes show high elastic modulus and good mechanical stability.[10,12–15]

Owing to the Pt-like d-band electronic structure and multiple oxidation states, Mo-based materials display high electrical

C. S. Rout, A. Patra
Centre for Nano and Material Sciences
Jain Global Campus
Jain (Deemed-to-be University)
Kanakapura Road, Bangalore, Karnataka 562112, India
E-mail: r.chandrasekhar@jainuniversity.ac.in
C. S. Rout, S. M. Jeong
Department of Chemical Engineering
Chungbuk National University
Cheongju, Chungbuk 28644, Republic of Korea
E-mail: smjeong@chungbuk.ac.kr
P. V. Shinde
Department of Molecular Sciences and Nanosystems
Ca' Foscari University of Venice
Via Torino 155, Mestre 30172, Italy

The ORCID identification number(s) for the author(s) of this article can be found under https://doi.org/10.1002/advs.202308178

DOI: 10.1002/advs.202308178

conductivity, optimal adsorption of intermediate, flexibility, strength, optoelectronic properties, etc. making them ideal candidates for various applications in sensing, catalysis, energy harvesting, electronics, energy storage, ion transport, superconductivity and hydrogen storage etc.[1,11,16] In the past few years, 2D metal borides with covalent networks have also enticed great interest since most of them are metallic leading to be highly conductive for fast electron transport and abundant catalytically active edges guarantee higher electrocatalytic activity than the corresponding bulk. As a d-block element with multiple oxidation states, molybdenum-based borides show properties such as low cost, facile synthesis, structural diversity, high chemical stability, corrosion resistance, high hardness, and capability to replace precious metal catalysts.[17–20] Molybdenum-based borides (molybdenum borides) are found in different stoichiometries and crystal structures namely α-MoB, Mo_2B, β-MoB, α-MoB_2, β-MoB_2, Mo_2B_4, and Mo_2B_5, etc.[5,19–22] The abundant structures of Mo borides represent interesting chemical and mechanical properties which are established by the rearrangement and proportion of boron and molybdenum atoms in a unit cell.[23,24] Due to the peculiar crystal structure and presence of unsaturated edge sites, molybdenum boride-based nanomaterials have both good conductivity and abundant catalytically active sites rising from the serious electron deficiency of boron atoms.

In this timely review, we aim to provide a comprehensive overview of the recent development and future perspectives of molybdenum borides and MBenes for various applications (**Figure 1**). This review will undoubtedly aid researchers in understanding the general state of these materials and will stimulate more effort devoted to this field. We begin with a brief introduction of molybdenum borides borides and MBenes including their structures, electronic and physicochemical properties, and synthesis approaches. Then, we present the most recent advancements in a variety of applications for these novel materials, such as energy storage (battery and supercapacitors), energy conversion, catalysis, lubrication, biosensor and surface-enhanced Raman spectroscopy (SERS), etc. In the end, comments and viewpoints on current difficulties, challenges, and future perspectives of materials are presented.

2. Typical Structure and Electronic Features

2.1. Structural Features

Molybdenum borides can be classified into three major types depending on the Mo and B molar ratios:[25] i) When the molar ratio Mo/B <0.5, the boron-rich borides show the structure of a 3D framework without metal-metal bonds; ii) For the molar ratio Mo/B >2, the metal-rich borides exhibit metal structure without boron-boron bonds; iii) For the moderate molar ratio ($0.5 \leq M/B \leq 2$), many bonds are possible and usually boron atoms construct a low dimensional substructure (boron dumbbells, boron chains, and boron layers). **Figure 2a** shows the crystal structures of the Mo-B system with the information about their space groups and Figure 2b summarizes the calculated energies of formation of the stable and metastable phases.[26–28] For the metal-rich molybdenum boride, the Mo atoms are bonded together to form a 3D metal skeleton, whereas the boron atoms/pairs are dispersed in the metal skeleton by Mo—B bonds.[1,3] In mono borides such as Mo—B, the metal atoms are arranged similarly to the elemental metals, while the boron atoms are inserted into the gap causing some expansion of the lattice. MoB and Mo_2B_2 are known to belong to the MBene family and are reported to be prepared from MoAlB by selective etching of Al layers.[29] MBenes are the class of orthorhombic and hexagonal 2D transition metal borides obtained from MAB phases with a chemical formula of M_nB_{n-2}. In the case of Mo-based MBenes, the crystal structure is the alternate stacking of the metal (Mo) and B layers and they can be classified into two categories: orthorhombic MBenes (ortho-MBenes) and hexagonal MBenes (hex-MBenes). Molybdenum diborides exist in two forms known as α-MoB_2 and β-MoB_2. In α-MoB_2, boron atoms are arranged into 2D graphitic boron layers whereas in β-MoB_2 they form puckered boron layers (Figure 2c).[2,3,30] α-MoB_2 is an AlB_2-type crystal phase structure, with alternating planar sheets of metals and boron atoms in sequences AHAHAHAH... β-MoB_2 is considered as the Mo_2B_5-type structure with AHA K BHB K CHC K A... arrangements (Figure 2c), where A, B, C are close-packed Mo layers; layers B and C are shifted by (a/3, 2a/3) and (2a/3, a/3) relative to A respectively and H is the graphite type layer constituted by B_1 atoms. The K-type layer is a puckered and densely packed boron network consisting of B_2 and B_3 atoms. In the case of boron-rich systems [MoB_3, MoB_4, and MoB_5, etc.], boron cages/clusters act as the structural units and are formed by the covalent bonds between boron atoms and connected further to form 3D boron skeleton. The metal atoms are inserted in the void of boron skeletons, which give additional valence electrons for the boron structural unit lacking electrons.

2.2. Electronic Features

Due to the diversity in the compositions of molybdenum borides, they can be arranged in varieties of crystal structures and possess different physical, and electronic properties. Further, their properties can be varied by non-stoichiometry or by incorporation of impurities.[4,31] The calculated electronic band structures of different molybdenum boride mono layers show Fermi level crossing of several bonds indicating excellent metallic behavior of the MoB_x (x = 1, 3, 4 monolayers) (**Figure 3a–c**).[27] The theoretical studies have confirmed that stable adsorption of Li atoms as the impurity is possible from different positions of the MoB_x layers (Figure 3d). The Li adsorption resulted in charge transfers of 0.85–0.88 e^- demonstrating its suitability for energy storage applications. Electronic structure calculations of Mo_2B revealed its typical metallic and non-magnetic nature with the negligible effect of native defects, biaxial tensions, and compressions on its properties.[32] Due to the low-frequency vibrations of the Mo atoms and the electronic occupations of the Mo-4d orbitals of tetr- and tri-Mo_2B_2 near the Fermi level, it shows intrinsic phonon superconductivity with a superconducting transition temperature (T_c) of 3.9 and 0.2 K respectively.[33]

3. Synthesis of Molybdenum Borides

Molybdenum borides can be synthesized by various physical and chemical methods including traditional solid-state, high-temperature, and/or high-pressure methods. These methods

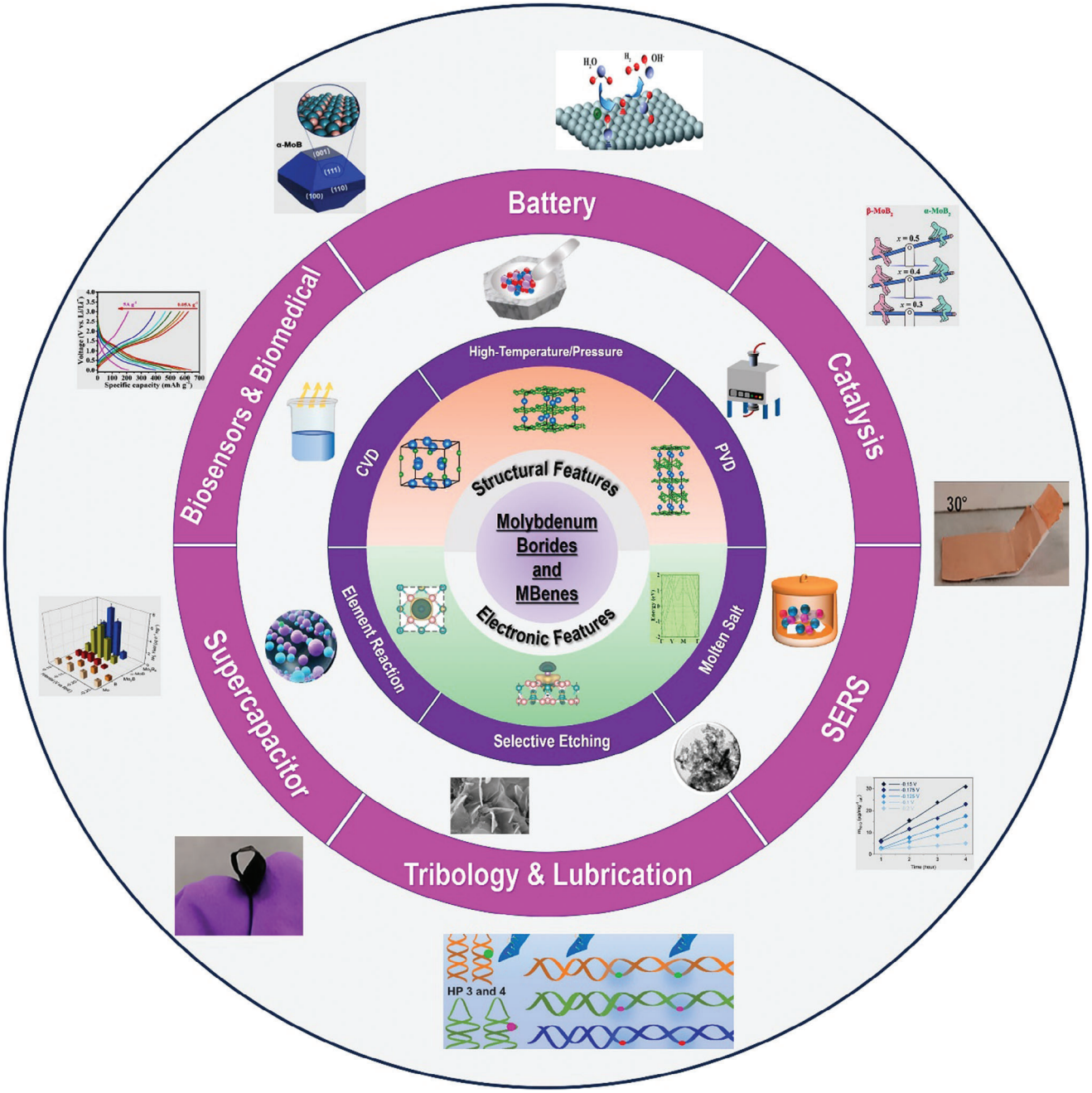

Figure 1. Schematic representation of preparation, properties, and recent developments of molybdenum-based borides and MBenes.

are physical vapor deposition (PVD), chemical vapor deposition (CVD), element reaction route, molten salt-assisted, and selective etching method.

3.1. High-Temperature and/or High-Pressure Methods

Molybdenum borides (Mo_2B, MoB, Mo_2B_5, MoB_4, MoB_2, etc.) can be synthesized by high temperature (>1200 K) and by high pressure (≈5.2 GPa) sintering (**Figure 4a**).[4,17,34] It is reported that by annealing the varied mixture of B/Mo precursor (molar ratio: 0.5, 1.0. 2.5, 4, etc.) in the presence of appropriate carbonization/decarbonization agent (Ca, Al, and Mg), different phases of molybdenum borides (Mo_2B, MoB, Mo_2B_5, MoB_4, MoB_2, etc.) with controlled size can be prepared.[35–38] In these high temperature-based approaches, boro/carbothermal reduction processes occur for the synthesis of the high entropy boride powders. However, these methods have several demerits since obtained products usually contain mixed phases with uncontrolled crystallization and large particle size.[38] The element

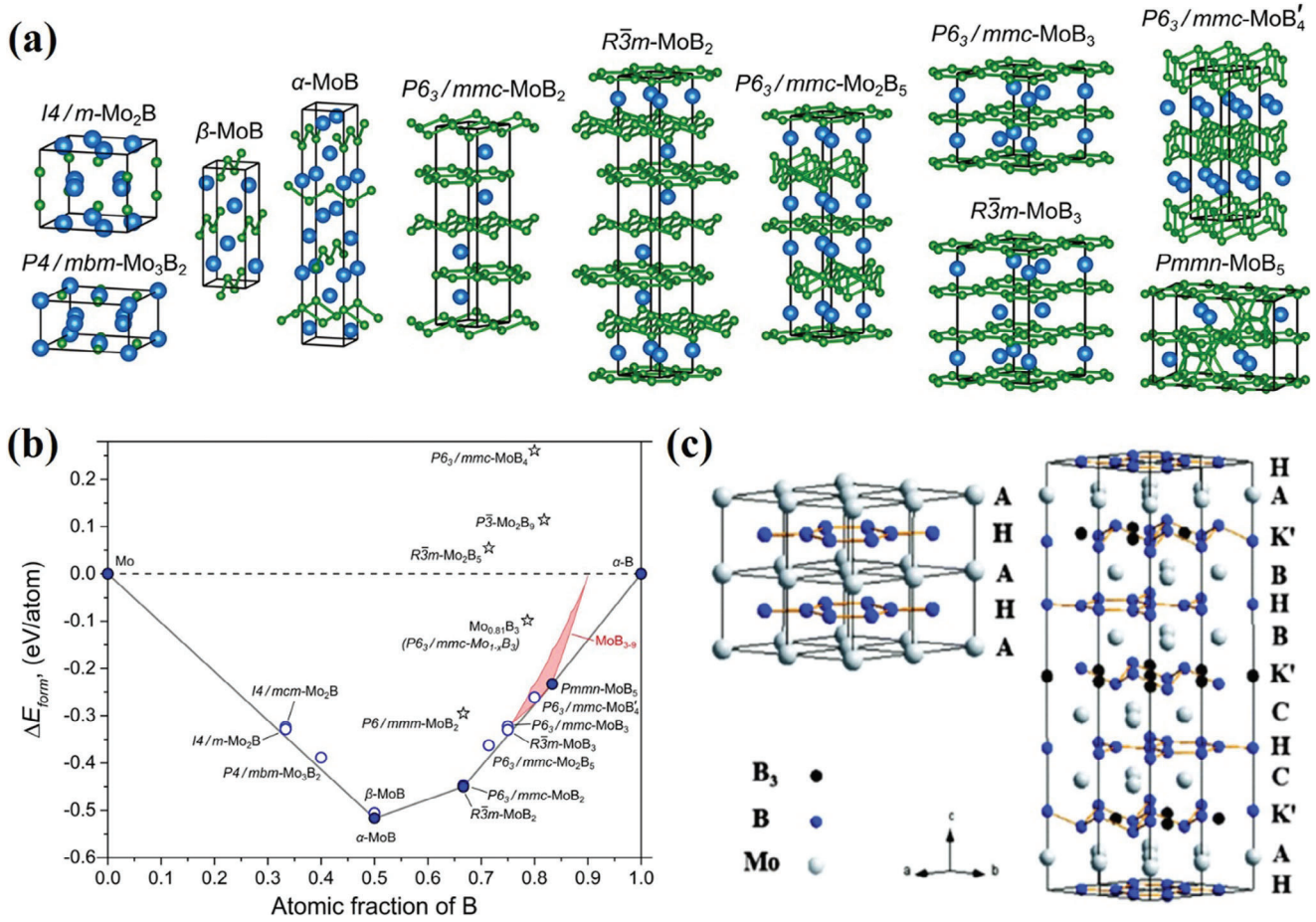

Figure 2. a) The Mo-B phases' crystal structures obtained by an evolutionary crystal structure search; b) Calculated formation energies for the Mo-B system. Stable and metastable phases are indicated by filled and hollow circles, respectively. The formation energy of the Mo-B structures suggested in the experimental investigations is displayed by stars. The shaded area portrays the energies of the formation of boron-rich MoB_x phases with $3 \leq x \leq 9$, obtained using a parameterized lattice model. Reprinted with permission.[26] Copyright 2020. American Chemical Society. c) Crystal structures of α-MoB_2 (*P6/mmm*) structure with ...AHAHAH... stacking sequence and β-MoB_2 (*R-3m*) structure with ...AHA K′ BHB K′ CHC K′ A... stacking sequence. Reprinted with permission.[30] Copyright 2013. Royal Society Chemistry.

reaction route is the common method for molybdenum boride synthesis in which the sintering of molybdenum and boron mixture in vacuum or inert gas is carried out under rigorous circumstances in a high-temperature instrument or arc-melting chamber.[20,39] Chen et al. reported the synthesis of several Mo-B phases with different crystal structures such as Mo_2B, MoB, α-MoB_2, and β-MoB_2 at high pressure of 5.2 GPa and high temperature of 1600–1800 °C.[20] Park's group employed an arc-melting method to synthesize Mo_2B, α-MoB, β-MoB, and α-MoB_2.[19] Further, it is demonstrated that the use of Sn flux promoted the reactivity and diffusion of solid reactants leading to the formation of single-phase Mo_2B_4 material.[21] Nguyen et al. prepared the molybdenum boride powder by a cost effective and simple pulsed discharge of compacted crystalline and amorphous micron-sized B powder.[39] In this method, the raw material (Mo rod and B micron-sized powder) was heated by a large pulsed current of electrical energy stored in capacitors. The vapor diffused with the vaporized/melted precursors formed the nanoparticles through a series of processes such as supersaturation, nucleation, and condensation (Figure 4b).[39]

3.2. PVD and CVD

PVD is the direct method for the synthesis of molybdenum borides without using any chemical etching and no involvement of chemical reactions.[40–42] PVD method offers distinct advantages in controlling the synthesis and structure of MBenes, thereby influencing their electrical behavior. PVD-grown MBenes typically exhibit high electron mobility and excellent conductivity due to the well-defined crystalline structures achieved during the deposition process. Sahu et al. reported the growth of 2D MoB MBene domains in a MoAlB thin film by Al deintercalation from MoAlB in the vicinity of AlO_x region via direct current magnetron sputtering (DCMS).[42,43] CVD is one of the controlled synthesis approaches to prepare molybdenum borides by heating the borane or a mixture of boron and its oxide as the boron source, Mo metal as the metal source, and hydrogen as the carrier gas and reducing gas.[44–48] Conversely, CVD-grown MBenes often demonstrate superior tunability and scalability, attributed to the precise control over growth parameters and defect engineering facilitated by the chemical nature of the deposition

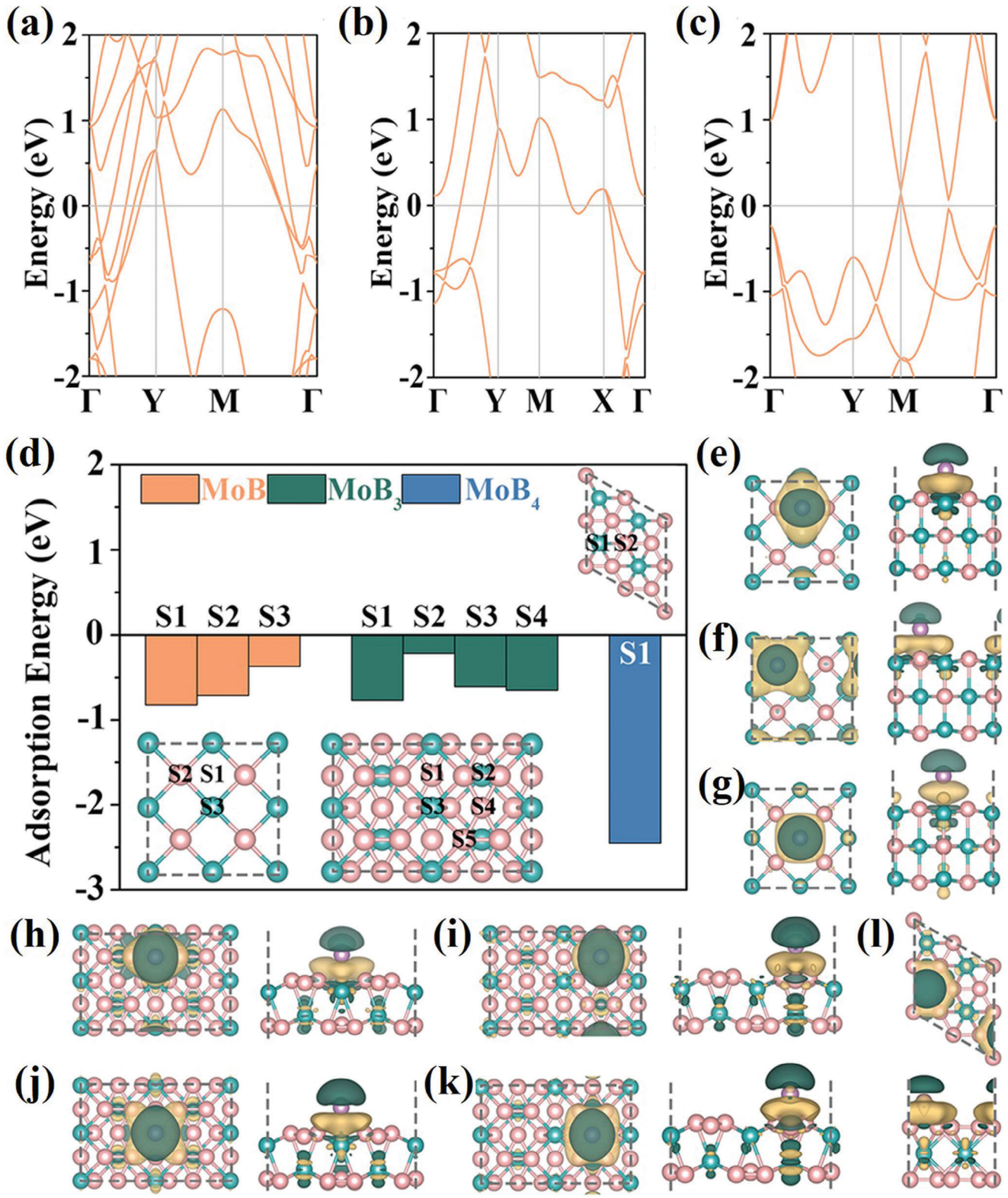

Figure 3. a–c) Electronic band structures of the MoB_x (x = 1, 3, and 4) monolayers; d) Adsorption energies of Li on the MoB_x (x = 1, 3, and 4) monolayers. The insets show the considered adsorption sites. Top and side views of the charge redistributions induced by the interaction of Li at the e) S1, f) S2, and g) S3 sites with the MoB monolayer, by the interaction of Li at the h) S1, i) S2, j) S3, and k) S4 sites with the MoB_3 monolayer, and by the interaction of Li at the l) S1 site with the MoB_4 monolayer. Green and yellow isosurfaces (isovalue: 0.01 electrons $Å^{-3}$) represent charge depletion and accumulation, respectively. Reproduced under terms of the CC-BY 4.0 license.[27] Copyright 2022. Springer Nature.

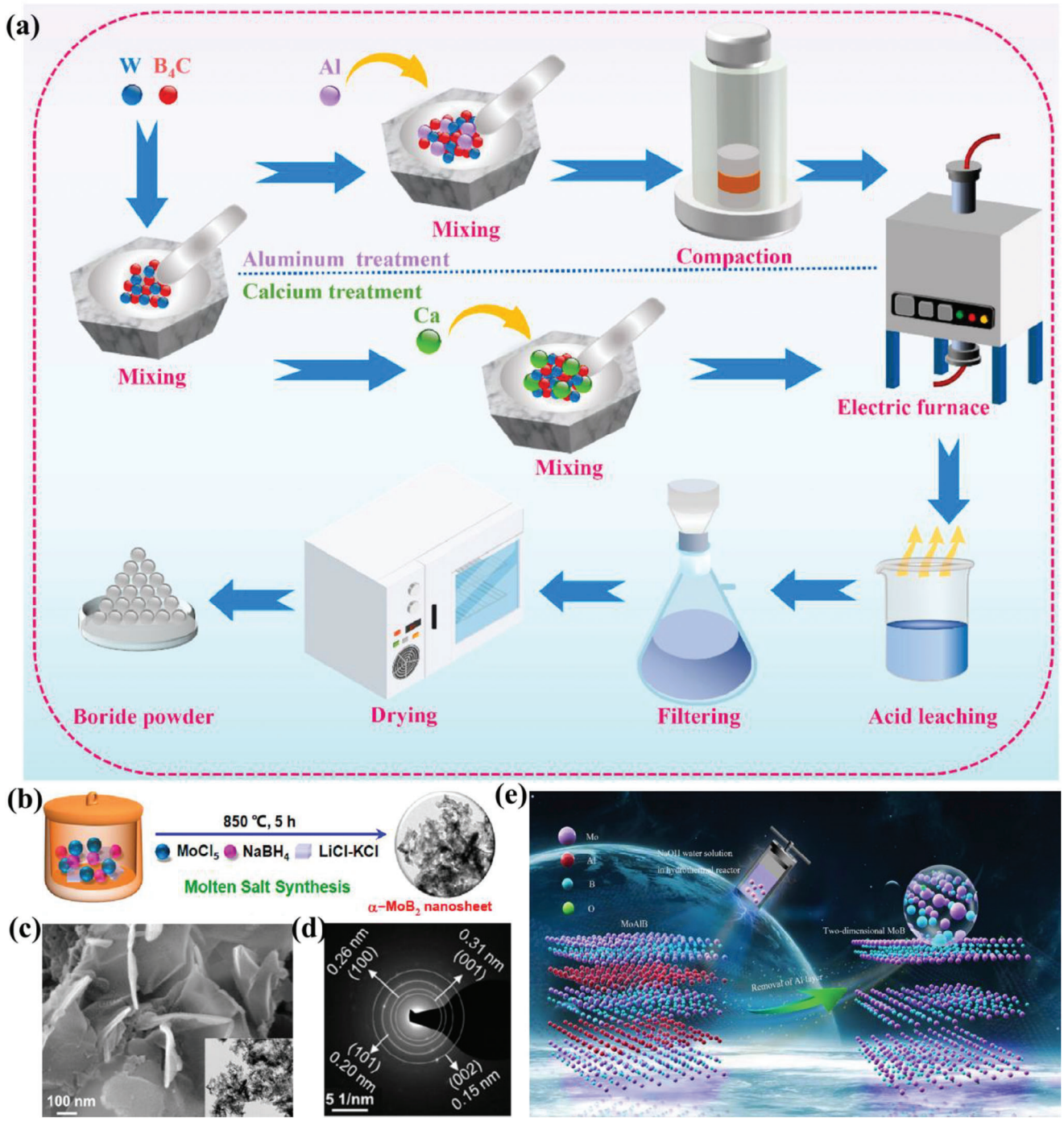

Figure 4. a) Schematic represents the preparation process of borides. Reprinted with permission.[34] Copyright 2023. Elsevier, b) Schematic representation of the preparation of α-MoB_2 nanosheets by the molten salt method, c) SEM and transmission electron microscopy (TEM) images of α-MoB_2 nanosheets, d) Selected area electron diffraction (SAED) pattern for the α-MoB_2 nanosheets. Reprinted with permission.[18] Copyright 2022. American Chemical Society. e) The schematic of the preparation of 2D MoB Mbene. Reprinted with permission.[48] Copyright 2022. Elsevier.

process. Comprehending the intricate interaction between deposition methods and the consequent electrical characteristics is vital for enhancing the performance of MBene-based electronic devices across a wide array of applications, spanning from flexible electronics to quantum computing. By this approach, Wang et al. obtained large area, ultra-thin, and highly conducting metallic hexagonal Mo_3B film.[5] Si et al. demonstrated a chemical potential modulated strategy to realize the precise synthesis of various ultra-high purity ultra-thin molybdenum borides by the CVD method.[49]

3.3. Molten Salt Method

The molten salt-assisted route is a promising approach with control over the phase formation and morphology to avoid excessive grain growth and high crystallinity.[50,51] Jothi et al. reported the synthesis of molybdenum mono borides (α-MoB) and molybdenum diborides (MoB_2 and Mo_2B_4) by using anhydrous Mo-Cl_5 and elemental boron in the presence of Sn metal precursor.[38] at high temperature (800−900 °C for 8 h). Liu et al. reported the synthesis of single-phase polycrystalline α-MoB_2 with nanosheet morphology through the $MoCl_5$ and $NaBH_4$ reaction in the LiCl-KCl molten salt (Figure 4c).[18] By changing the "B" precursor to "B" powder β-MoB_2 was achieved under similar experimental conditions.[52]

3.4. Selective Etching Method

Similar to MXene synthesis from the MAX phase by etching of "A" element, MoAlB etching is reported by different etchants such as NaOH, HF, and LiF in HCl.[46,53,54] However, it is observed that the metastable phase Mo_2AlB_2 emerges during topochemical de-intercalation of Al from MoAlB, and complete etching of Al is found to be difficult.[54] A schematic in Figure 4d shows the fabrication process of 2D MoB MBene through a hydrothermal-assisted alkane solution etching strategy.[46] The pristine MoAlB exhibits a lamellar-stacking structure, whereas MoB particles exhibit accordion-like layer structure like MXene materials. It is reported that MBenes could not be directly obtained from MoAlB because of a structural difference in the Al layers between MAX and MAB phases, i.e., MAX phases contain a single Al layer while MAB has a zigzag double Al layer. Due to this reason, partially "Al" etched MBenes are represented as $MoAl_{1-x}B$.[55] Zhou et al prepared boridene (2D molybdenum boride sheets) with ordered metal vacancies, $Mo_{4/3}B_{2-x}T_z$ by selective etching of aluminum and yttrium or scandium atoms from 3D in-plane $(Mo_{2/3}Y_{1/3})_2AlB_2$ and $(Mo_{2/3}Sc_{1/3})_2AlB_2$ in aqueous hydrofluoric acid.[56] The sheets may have a minor B deficiency, with x up to ≈0.5, in comparison to the parent phase. The surface terminations T_z were found to be a mixture of O, OH, and F, with z ranging from 2 to 3. Majed et al. prepared the Mo_2AlB_2 phase by partial selective etching of Al from the MoAlB phase using HF acid at 45 °C for 48 h (**Figure 5a**).[57] The (020) reflection shift due to etching from 12.6° (2θ) to 13.8° (2θ), signifying a reduction in d-spacing from ≈7.0 to 6.4 Å and removal of an Al layer (Figure 5c).

4. Applications of Molybdenum Borides and MBenes

Due to their several advantages including high chemical, mechanical, and thermal stability, molybdenum borides-materials have emerged as the ideal candidate for a wide range of applications in electrochemical energy storage, catalysis, biosensors, tribology, and high-temperature structures in the aerospace industry.[46,55,57] In this section, we will discuss the recent applications of these materials in different fields (**Figure 6**).

4.1. Energy Storage Devices

Mo borides and 2D MBenes have gained interest in energy storage applications due to their several unusual physicochemical properties with key advantages such as large surface area, active edge sites, high mechanical properties, flexibility, etc.[20,44,58–62]

4.1.1. Battery

Theoretical predictions showed that molybdenum borides and MBenes have inherent mechanical anisotropy and metallic properties, low diffusion potential, and low open circuit voltage.[63] The predicted properties of these materials suggested that they can be attractive anode materials for Li/Na ion batteries.[63] Wang et al. showed that Li and Na possess negative adsorption energies when interacting with Mo_2B, which could prevent the formation of metallic Li and Na and improve safety and reversibility when used as anodes in ion batteries.[32] The diffusion barriers for Li (Na) ions in 2D Mo_2B are reported to be 0.073 (0.069) eV and the open circuit voltages are 0.62−1.15 (0.42−1.41) V respectively. T-type Mo_2B is found to show high theoretical volumetric capacity (≈2424 $mAhcm^{-3}$) with low energy barriers (0.0372 eV) as compared to the H-type Mo_2B.[64] Similarly, MoB and MoB_3 monolayers are found to be good anode materials of Li-ion batteries with Li specific capacities of 670 and 418 $mAhg^{-1}$ with low Li diffusion barriers of 0.10 and 0.13 eV respectively.[27] Strong mechanical and thermal properties and high in-plane stiffness of pristine and lithiated MoB_2 demonstrated that it can withstand massive volume expansion at 500 K during lithiation/de-lithiation reactions, which is remarkably beneficial for the manufacturing of flexible anodes.[65] Tetragonal and trigonal Mo_2B_2 displayed excellent electronic conductivity and great stability for the Li and Na ion battery applications with specific capacity values in the range of ≈251 and 188 $mAhg^{-1}$ respectively.[66,67] Recently, experimental results on molybdenum boride and MBenes-based materials are demonstrated as promising candidates for the anodes of Li-ion batteries.[68–70] 2D MoB MBene etched from MoAlB exhibited a reversible specific capacity of 144.2 $mAhg^{-1}$ after 1000 cycles at the current density of 2 Ag^{-1}.[46] Figure 6 shows the electrochemical performance of MBene-based anodes in Li-ion batteries. Ex situ X-ray diffraction (XRD) and field emission scanning electron microscopy (FESEM) analysis of the electrodes after long cycling studies showed no noticeable change in the material in terms of its crystal structure and morphology. In situ, XRD results during the charging/discharging processes confirmed that MBenes are not electrochemically active and the formation of Li-MoB phase occurs during lithiation/de-lithiation (Figure 6). The Mo_2AlB_2 shows a higher specific capacity (593 $mAhg^{-1}$ at 200 mAg^{-1} after 500 cycles than MoAlB electrodes.[57] It is further confirmed that surface redox reactions are responsible for Li storage in $MoAlB_2$ rather than intercalation or conversion processes. Due to the good hydrophilic properties and good wettability toward electrolytes of MoB, the Li-S batteries based on these electrodes displayed impressive electrochemical performance with a high capacity of 1253 $mAhg^{-1}$ and a long life span (1000 cycles).[68] **Table 1** summarizes the battery applications of different Mo borides and MBenes.[46,57,68,69]

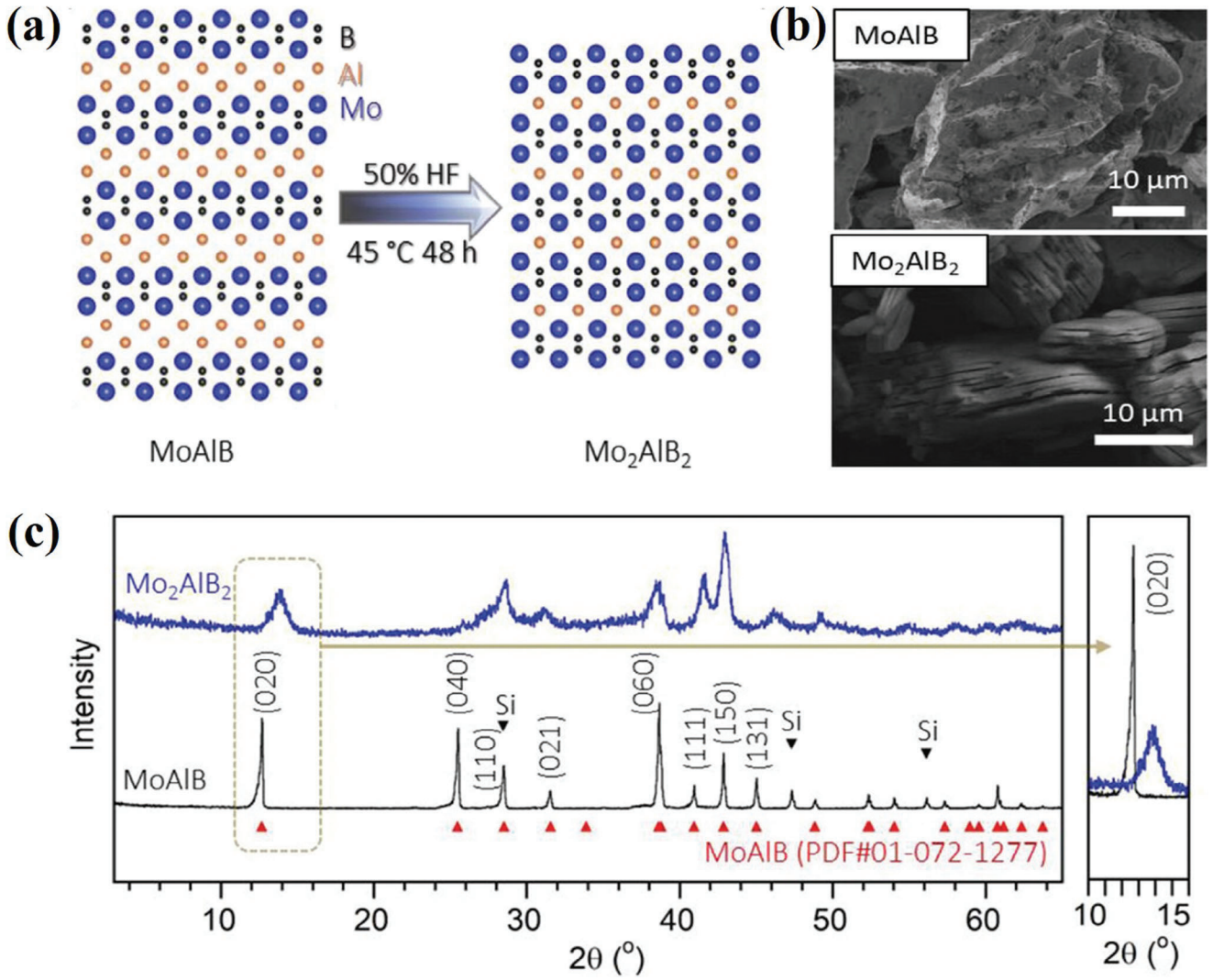

Figure 5. a) Schematic for the structural evolution of Mo_2AlB_2 from MoAlB, b) SEM of MoAlB before and after etching, c) XRD of MoAlB before and after HF treatment. Reprinted with permission.[57] Copyright 2023. Wiley.

4.1.2. Supercapacitors

To date, only a limited number of MBenes have been employed as electrode materials for supercapacitors. However, Mo_2B_2 and its derivatives show promise for energy storage applications due to their notable properties such as high conductivity, electrochemical surface area, and surface roughness. This suggests that Mo_2B_2-based materials could be particularly effective in enhancing the performance of supercapacitors by facilitating efficient charge transfer and storage processes. Partially "Al" etched MoAlB nanosheets are reported to show good energy storage performance when used as the electrodes of supercapacitors (Table 1).[70–72] 2D MBenes applied as the pseudocapacitive filter electrochemical supercapacitor electrode material exhibited excellent AC filtering performance with a specific capacitance of 702 $mFcm^{-2}$ under the AC condition of 120 Hz and a negative phase angle of 54.8°.[70] All-solid-state supercapacitors based on multilayered MBenes delivered significant capacitance, high energy density, and power density even at a 90° bending angle (**Figure 7**).[71] Vinoth et al. demonstrated the asymmetric supercapacitors based on MoB nanosheets and activated carbon as the electrodes with 1 M H_2SO_4 and 1 M Na_2SO_4 as the electrolytes.[72] The asymmetric device delivered a high energy density of 14 $WhKg^{-1}$ at a power density of 16.8 $kWKg^{-1}$.

4.2. Catalysis

Mo borides and 2D MBenes have shown promising electrocatalytic activities toward various reactions due to the broad specific surface area, diverse surface chemical composition, and metallic conductivity.[1,2,25]

4.2.1. Hydrogen Evolution Reaction (HER)

In recent years, HER has become one of the most studied research topics due to its highly promising technological charac-

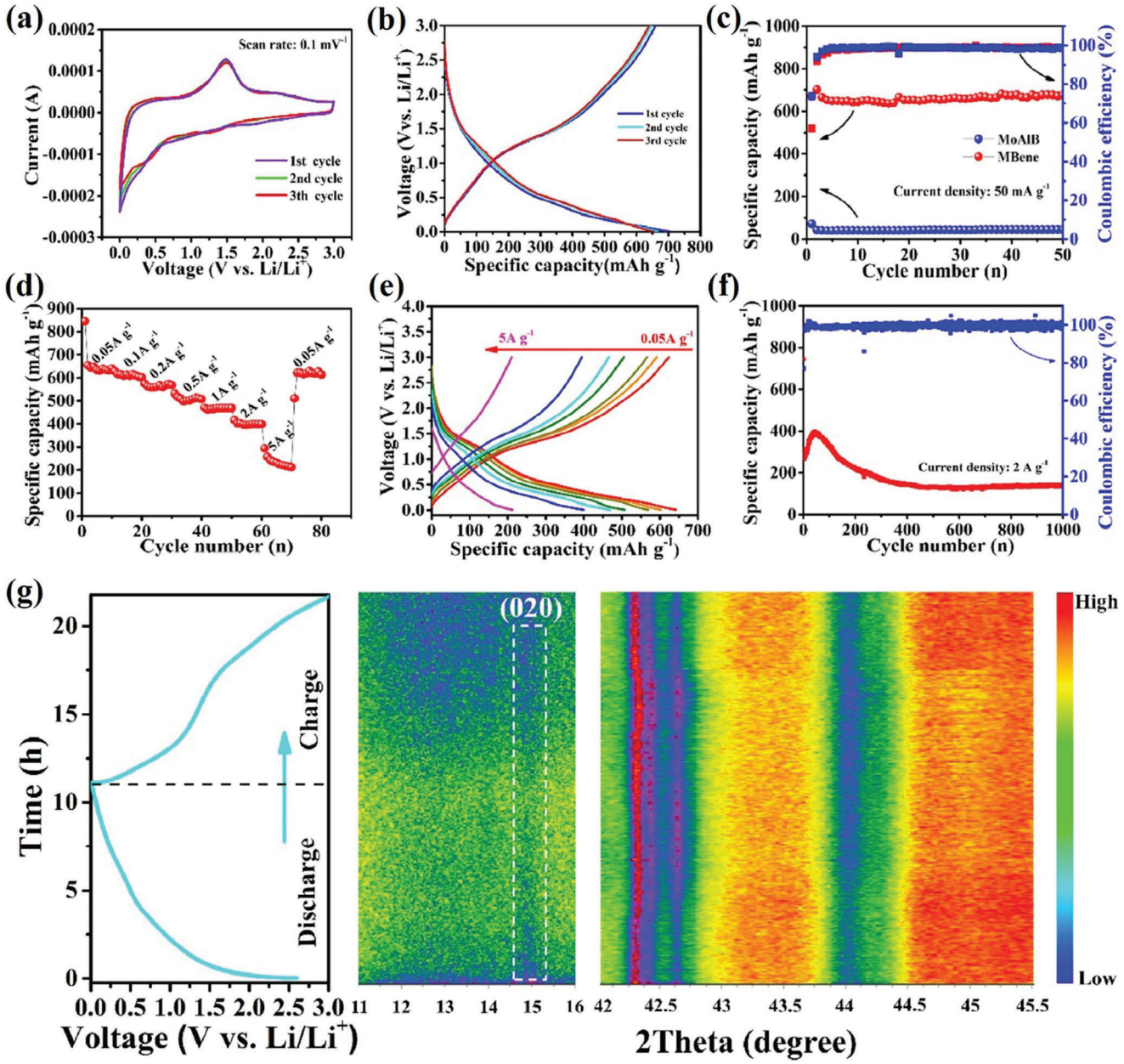

Figure 6. Performance of the 2D MoB MBene anodes in lithium-ion batteries, a) Cyclic voltammetry (CV) curves at a scan rate of 0.1 mV $s^{-1,}$ b) Charge–discharge curves at 50 mA g^{-1},c) the cycle performance of MoAlB and 2D MoB MBene at 50 mA g^{-1} d) rate capability, e) the corresponding voltage curves of 2D MoB MBene, f) long cycle performance at 2 A g^{-1},g) In situ XRD plots with the corresponding discharge–charge curve. Reprinted with permission.[46] Copyright 2022. Elsevier.

teristics for sustainable and large-scale hydrogen production capability. A comparative study of the HER activity of Mo_2B, α-MoB, β-MoB, and MoB_2 demonstrated that MoB_2 and β-MoB exhibits excellent activity whereas the molybdenum-rich Mo_2B shows significantly lower activity.[19,49] But in another report, the CVD-grown Mo-rich ultrathin Mo_3B films of 6.48 nm thickness on Mo foils exhibited fantastic stability and a lower Tafel slope of 52 $mVdec^{-1}$.[5] Theoretical studies showed the metallic nature and the faster electron transport along the active edges of the thin films helped to achieve better catalytic properties. The density functional theory (DFT) calculations on free energy revealed that the active sites in the graphene-like B-layer contribute to the high HER activity as compared to the phosphorene-like B-layer in Mo_2B_4.[21] Further, comparative theoretical studies on the HER activity confirmed that the performance increases with increasing boron content from Mo_2B (no B—B bonds are less active) to α-MoB and β-MoB (zigzag boron chains are intermediate active) and MoB_2 (planar graphene-like boron layers are more active).[73] Further, it is demonstrated that the (001) boron layer in hexagonal MoB_2 (α-MoB_2) is the most active (with performance in the range of Pt (111) surface and the puckering this flat boron layer to the chain-like configuration (phosphorene like layer; β-MoB_2

Table 1. Recent literature on the battery and supercapacitor applications of molybdenum borides and MBenes.

Application/Materials		Performance		Ref.
Battery	Ion battery type	Reversible capacity ($mAhg^{-1}$)	Rate and cycling capability	
MoB	Li	701 $mAhg^{-1}$ at 50 mAg^{-1}	144.2 $mAhg^{-1}$ at 2 Ag^{-1} after 1000 cycles	[46]
$MoAl_{1-x}B$	Li	460 $mAhg^{-1}$ at 20 mAg^{-1}	209 $mAhg^{-1}$ at 1 Ag^{-1} after 500 cycles	[56]
MoB	Li-S	1253 $mAhg^{-1}$ at 0.5 C	1192 $mAhg^{-1}$ at 0.2 C after 350 cycles	[68]
Mo-MoB	Li-S	1188 $mAhg^{-1}$ at 0.2 C	672 $mAhg^{-1}$ at 0.2 C after 50 cycles	[69]

Supercapacitor	Type of supercapacitor device	Capacitance	Energy density at power density	Cycle test retention (%)/cycles	
MoB	AC filtering capacitors	702 μFcm^{-2}, Negative phase angle ≈ 54.8° at 120 Hz	–	–	[70]
MoB	All-solid-state supercapacitor	741.6 $mFcm^{-2}$ at 1 mVs^{-1}; stable performance even at 90° bending	24.65 $\mu Whcm^{-2}$ @ 2mWcm^{-2}	80.2%/ 5000	[71]
MoB	Asymmetric supercapacitor	445 Fg-1 at 1Ag^{-1} with 1.4 working window	14 $Whkg^{-1}$ @ 16.8 $kWkg^{-1}$	98%/ 2000	[72]

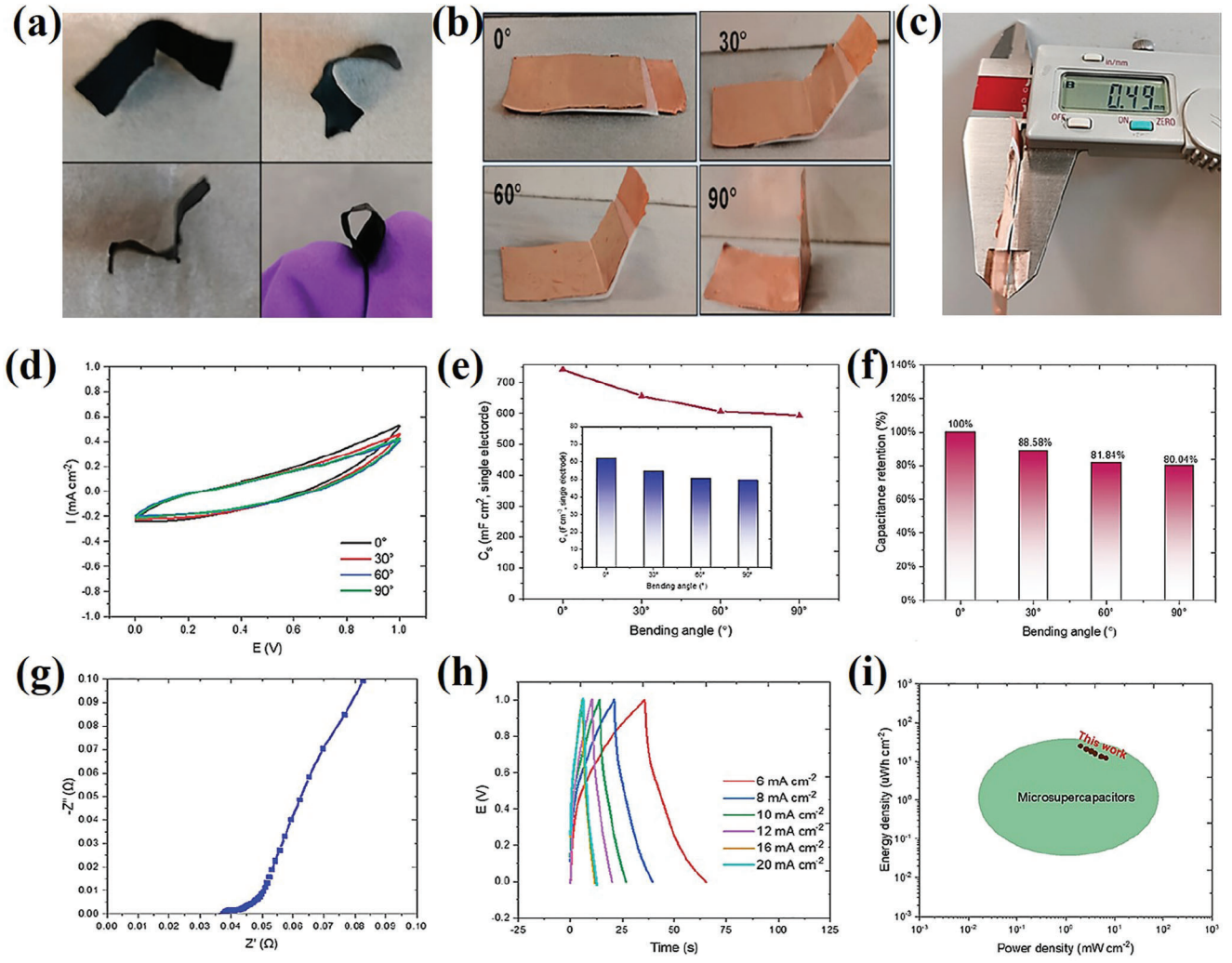

Figure 7. Fabrication and electrochemical measurements for 1/24-$MoAl_{1-x}B$ all-solid-state supercapacitor (ASSS), a) Photographs of a 1 × 1.5 cm^2 film electrode bent to various shapes, b) Photographs of ASSS bent to different bending angles (0, 30, 45, and 90°), c) Thickness of the fabricated ASSS, d) CV curves under different bending angles, e) capacitance under different bending angles, f) capacitance retention of the single electrode, g) Nyquist plots, h) Galvanostatic charge-discharge (GCD) curves, i) Ragone plots. Reprinted with permission.[71] Copyright 2023. American Chemical Society.

Table 2. Recent literature on the HER applications of molybdenum borides and MBenes.

[78] Catalyst	Method of preparation	Overpotential	Tafel slope ($mVdec^{-1}$)	Ref.
Mo_3B film (6.48 nm)	CVD	249 mV @ 20 $mAcm^{-2}$	52	[6]
Mo_2B_4 powder	High temperature (1100° C) sintering	270 mV @ 3.5 $mAcm^{-2}$	80	[21]
Downsized Mo_2B_5 powder (≈ 200 nm)	Downsized by electrochemical approach	740 mV @ 10 $mAcm^{-2}$	118.4	[22]
MoB	Commercial powder (High temperature)	301 mV @ 10 $mAcm^{-2}$	55	[74]
α-MoB_2	Molten salt method	124 mV @ 10 $mAcm^{-2}$	63	[18]
β-MoB_2	Molten salt method	187 mV @ 10 $mAcm^{-2}$	49.3	[52]
MoB_2 nanoparticles	Redox-assisted solid-state meta-synthesis reaction	154 mV @ 10 $mAcm^{-2}$	49	[75]
$Mo_{0.9}Ni_{0.1}B_2$	Molten salt technique	222 mV @ 10 $mAcm^{-2}$	68.4	[76]
Mo_2NiB_2	High temperature (1100 °C) vacuum annealing	160 mV @ 10 $mAcm^{-2}$	71	[77]
α-$Mo_{0.7}W_{0.3}B_2$	Arc melting method	201 mV @ 10 $mAcm^{-2}$	63.8	[78]
Pt-$MoAl_{1-x}B$	Selective Al etching and chemical method	32 mV @ 10 $mAcm^{-2}$	83.6	[55]
MoB/g-C_3N_4	Physical mixing of commercial MoB and g-C_3N_4 (prepared by thermal polymerization)	152 mV @ 20 $mAcm^{-2}$	46	[79]

or Mo_2B_4) leads to a reduction in the activity. The HER activities of various molybdenum-based borides produced through various techniques are listed in **Table 2**.[21,22,74–79] Recently, 2D MBenes prepared by partial etching of Al from MoAlB have been reported to show promising HER activity.[55,74,80–82] The overpotential of the partially etched $MoAl_{1-x}B$ is reported to decrease by 99 mV (i.e., 301 mV at 10 $mAcm^{-2}$) as compared to the non-etched crystals due to the increase in the surface area of exposed catalytically active basal planes.[82] Recent literature suggests that both α-MoB_2 and β-MoB_2 show promising HER activity in both acidic and alkaline media with good cycling stability.[18,75,83,84] Gong's group showed that α-MoB_2 and β-MoB_2 nanosheets deliver low overpotential of 124 and 187 mV at 10 $mAcm^{-2}$ with Tafel slope 63 and 49.3 $mVdec^{-1}$, respectively.[18,52] $Mo_{4/3}B_{2-x}T_z$ boridene prepared from borides ($(Mo_{2/3}Y_{1/3})_2AlB_2$ and $(Mo_{2/3}Sc_{1/3})_2AlB_2$) by selective etching showed an onset potential of 0.15 V with respect to the reversible hydrogen electrode.[85]

Tailoring the electronic structure by alternating crystal structure and incorporation of heteroatom lead to the reduction of ΔG_H* and thereby improve the HER activity of molybdenum borides.[76,78,86,87] Peighmbardoust et al. demonstrated that by doping transition metals to MoB_2 with varied concentrations (TM = Ni, Co; x = 0, 0.05, 0.1, 0.2, 0.3, 0.4, and 0.5), HER activity can be tuned.[76] $Mo_{0.9}Ni_{0.1}B_2$ afforded 10 $mAcm^{-2}$ at a low overpotential of 220 mV and the assembled $Mo_{0.9}Ni_{0.1}B_2$ (cathode)‖$Mo_{0.8}Co_{0.2}B_2$ (anode) couple demanded 1.75 V to produce 10 $mAcm^{-2}$ which was close to the value of the state-of-the-art Pt/C‖RuO_2 pair with Faradaic efficiency ≈80% (**Figure 8**). Park et al. showed that W doping in α-MoB_2 promoted hydrogen generation by facilitating bonding between hydrogen atoms in contrast to Mo. In another report, Dutta et al. showed Ni substituted cobalt molybdenum boride nanosheets show superior HER performance with a low overpotential of 69 mV at 10 $mAcm^{-2}$ and Tafel slope of 76.3 $mVdec^{-1}$ in alkaline medium.[88] Recently, it was reported that by minimum amount of Pt single atom catalyst loading to partially etched $MoAl_{1-x}B$, the HER activities impressively enhanced with a low overpotential of 32 mV and 18 mV at 10 $mAcm^{-2}$ in alkaline and acid media.[55] Zhang et al. demonstrated that by forming Schottky junctions of metallic MoB with n-type semiconductor g-C_3N_4, the HER catalytic activities can be optimized.[79] The MoB/g-C_3N_4 Schottky catalyst exhibited superior HER activity with a low Tafel slope of 46 $mVdec^{-1}$ and a high exchange current density of 17 μAcm^{-2}.

4.2.2. Nitrogen, Carbon Dioxide Reduction Reactions

Design and synthesis of efficient catalyst for electrochemical nitrogen reduction reaction (eNRR) with less energy consumption, lower CO_2 emission, high selectivity, and high NH_3 yield have gained tremendous interest.[89–91] By considering several advantages and better electrocatalytic properties, Peng et al. investigated molybdenum borides with various Mo-B stoichiometry ratios (Mo_2B, α-MoB, Mo_2B_4).[92] Mo_2B_4-based catalysis showed the highest NH_3 yield of 7.65 $\mu gh^{-1}/mg$ at −0.15 V with Faradaic efficiency (FE) of 12.47%, whereas α-MoB exhibited the fastest eNRR reaction with a higher FE of 17.7% (**Figure 9**). Further, DFT calculations revealed that due to the intermediate B content in α-MoB, the reaction intermediates were not able to bind not too weekly or too strongly, which helped to achieve the highest activity of eNRR. Similarly, CrB, MnB, MoB, HfB, and WB were employed as model catalysts to elucidate the associative and dissociative mechanisms of NO_x RR. The hydrogenation process involved two pathways: associative, where N—O bond activation occurred after adsorption, and dissociative, where immediate N—O bond breaking led to the formation of isolated N and O atoms on MBenes. This eventually converted into NH_3 and H_2O with the addition of $H^+ + e^-$.[93]

The potential of four 2D MBene nanosheets as catalysts for CO_2 reduction is quite notable. Mo_2B_2 and Cr_2B_2 emerged as promising candidates with notable catalytic selectivity, attributed to their subpar performance in HER and a low-limit potential for CO_2 reduction.[94,95] The study revealed that among the MBenes considered, Mo_2B_2 and Cr_2B_2 maintained a lower limit potential, recording values of −0.45 and −0.5 eV, respectively. Notably,

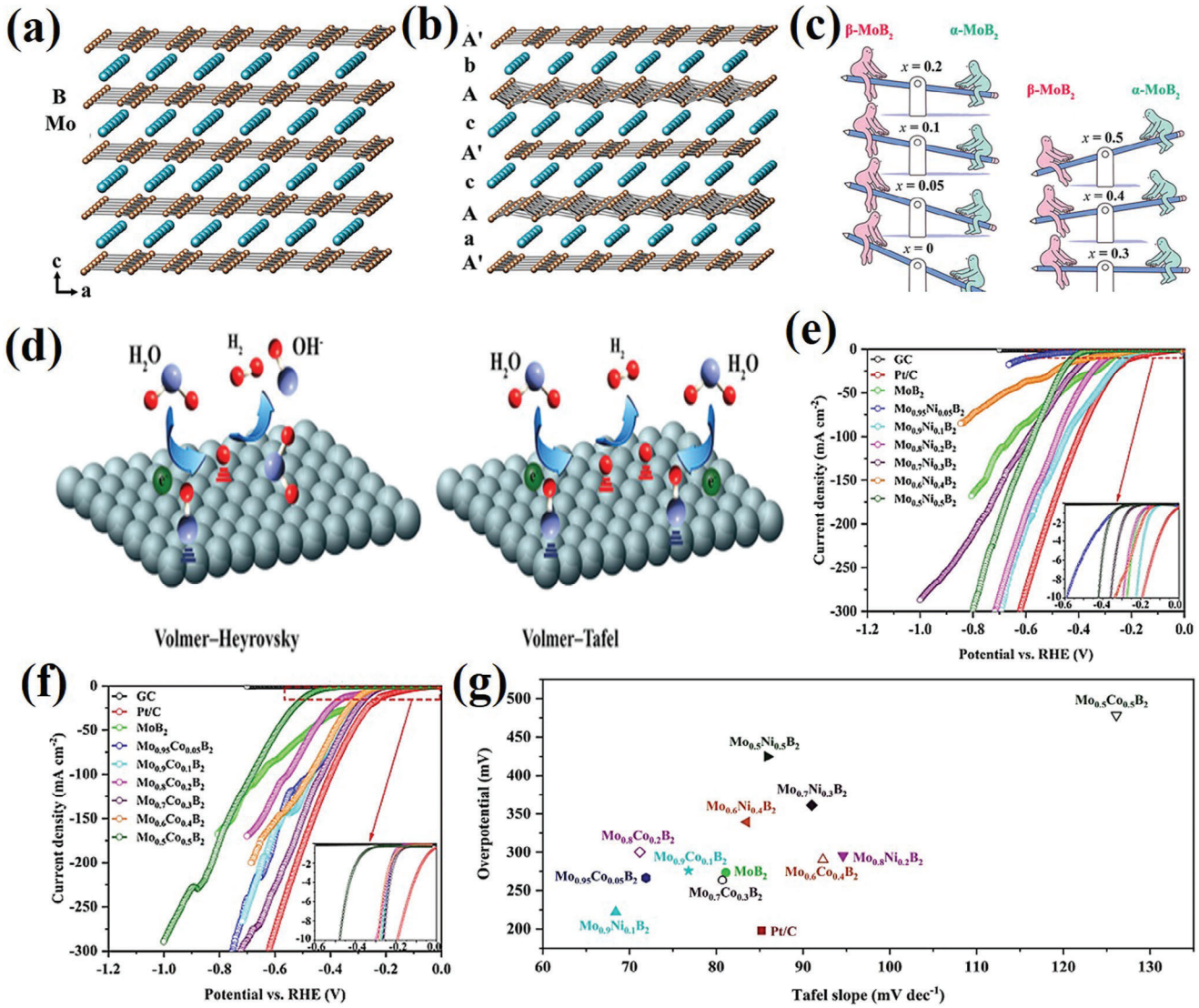

Figure 8. a) Crystal structures of AlB_2-type with flat boron layers (α-MoB_2), b) Crystal structures of rhombohedral R3m (β-MoB_2), c) Schematic represents the modification of the MoB_2 structure with varying substitution content (x), d) Volmer–Heyrovsky and Volmer–Tafel mechanisms of HER in alkaline solution, e) Linear sweep voltammetry (LSV) curves of Ni-substituted MoB_2 1.0 M KOH, f) LSV curves of Co-substituted MoB_2 1.0 M KOH, g) A comparison of the overpotential (at 10 $mAcm^{-2}$) and Tafel slope on various HER catalysts. Reprinted with permission.[76] Copyright 2022. American Chemical Society.

the analysis of Gibbs energy indicated that CHO formation exhibited the highest increase on all MBenes. Likewise, Xioa et. al. identified C1 hydrocarbon products, including CH_4, CH_3OH, HCHO, CO, and HCOOH, suggesting that these MBenes exhibit high stability, catalytic activity, and selectivity in the context of CO_2 reduction.[96] MoB is evaluated as a CO_2 reduction catalyst, outperforming traditional Mo_2C due to its metallic nature and excellent electrical conductivity. It effectively activates CO_2 with higher interaction energy (−3.64 eV), resulting in significant charge transfer. MoB exhibits superior catalytic selectivity by inhibiting the hydrogen evolution reaction and displaying low reaction energy. Particularly, at potentials below −0.62 V, MoB promotes a high-throughput CO_2 reduction process, favoring CH_4 production.[97,98]

4.3. Biochemical Sensing and Surface-Enhanced Raman Spectroscopy (SERS)

The combination of the unique optical, electronic, and catalytic properties of molybdenum boride has shown promising performance for its use in biomedical applications for miRNA detection.[99] Zada et al. demonstrated the ability for the monitoring of miRNA expression in living cells by Mo_2B nanosheets (**Figure 10**). Mo_2B nanosheets displayed strong interaction with the hairpin probes (HPs), ssDNA loop, and excellent multiple fluorescence quenching performance with ultra-low background signal. The biomarkers imaging successfully monitored the expression change of miRNAs in cancer cells which holds a promising role in biological and biomedical research.

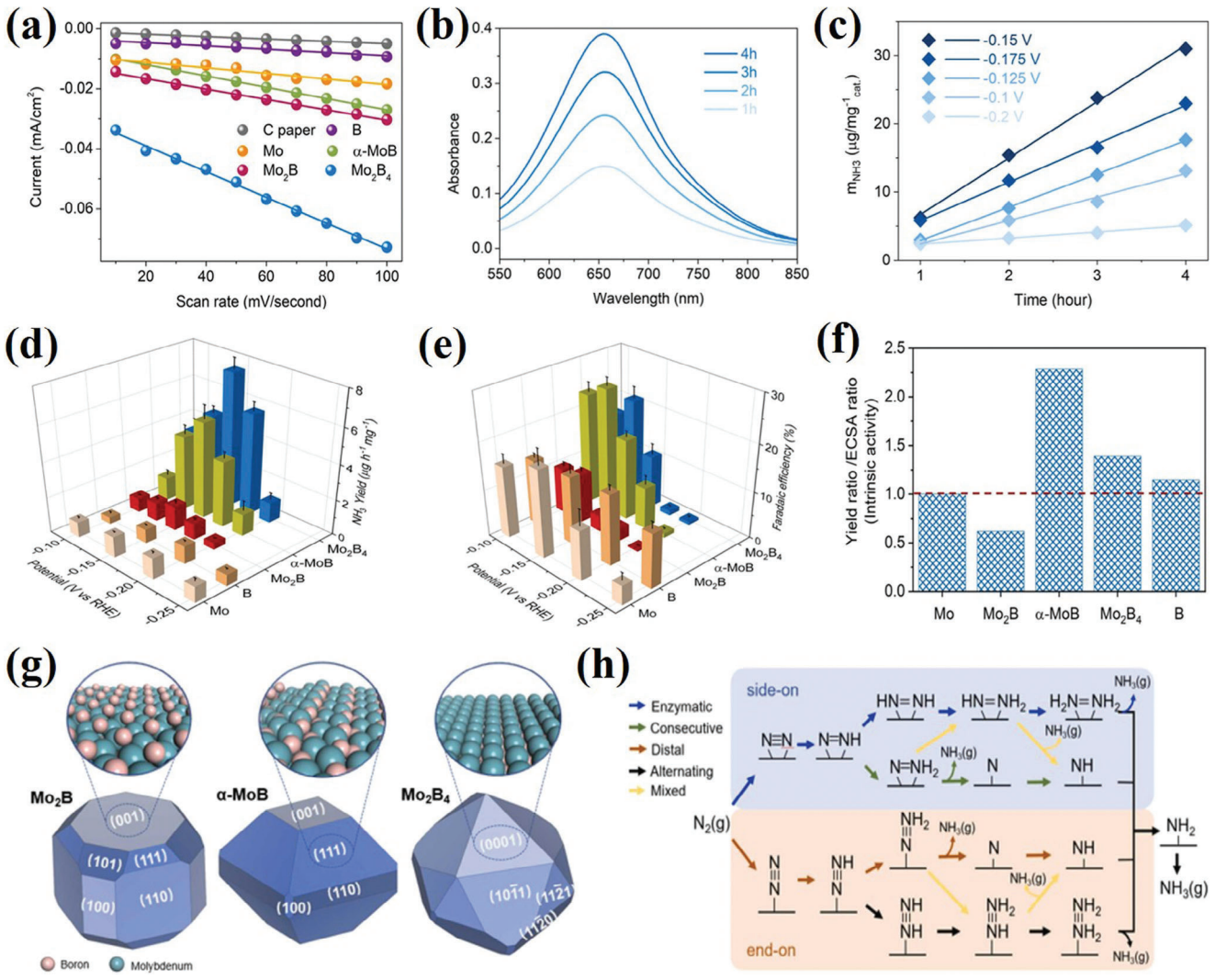

Figure 9. a) The cathodic charging currents of C paper, Mo, B, Mo_2B, α-MoB, Mo_2B_4 at 0.15 V versus RHE as a function of scan rates; b) Ultraviolet-visible spectra of the electrolyte stained with indophenol indicator by using Mo_2B_4 as a catalyst; c) Ammonia concentration in electrolyte as a function of time using Mo_2B_4 as a catalyst in N_2; d) Ammonia production yields; e) Faradaic efficiencies; f) The intrinsic activity of Mo, Mo_2B, α-MoB, Mo_2B_4, and B in terms of Yield ratio/ Electrochemically active surface area ratio (with respect to Mo); g) Wulff shapes of Mo_2B α-MoB, Mo_2B_4 determined by DFT calculations and corresponding most energetically stable surface structures; h) Scheme for the possible reaction mechanism of eNNR. Reprinted with permission.[92] Copyright 2023. Elsevier.

Pristine MBenes served as favorable adsorbents for capturing NO, SO, and CO. Conversely, functionalized MBenes-NH_3 systems exhibited moderate adsorption energies, indicating excellent sensitivity (< 0.5 eV) for NH_3 gas detection in both phases.[100] The optimization of fabrication parameters, functionalization strategies, and sensor configurations is essential for enhancing sensitivity while maintaining robustness and reliability in real-world applications. Specifically, 2H-Mo_2BH_2 demonstrated higher CT (−0.11e) and appropriate adsorption energy (−0.30 eV), resulting in a shorter recovery time of 12 µs. Additionally, density of states calculations indicated that the electrical conducting properties of MBenes make them well-suited for efficient NH detection with a brief recovery time.

Due to the multiple crystallographic arrangements, structural transformation, and metallic behavior, MBenes emerge as the ideal candidate for SERS due to the efficient photoinduced charge transfer (PICT) process between MBenes and the molecular level of the probe molecules.[101] 2D $Mo_{4/3}B_2$ MBene displayed higher SERS performance than majority of the semiconductor SERS substrates with a Raman enhancement factor of 3.88×10^6 and ultra-low detection limit of 1×10^{-9} M. DFT calculations confirmed that MBenes have the capability to achieve ultrahigh SERS sensitivity due to the availability of abundant electronic density of states near the Fermi level as compared to the bulk MoB.

4.4. Tribology and Lubrication

The application of efficient lubrication materials has an important role in different sectors such as aerospace, automotive, and

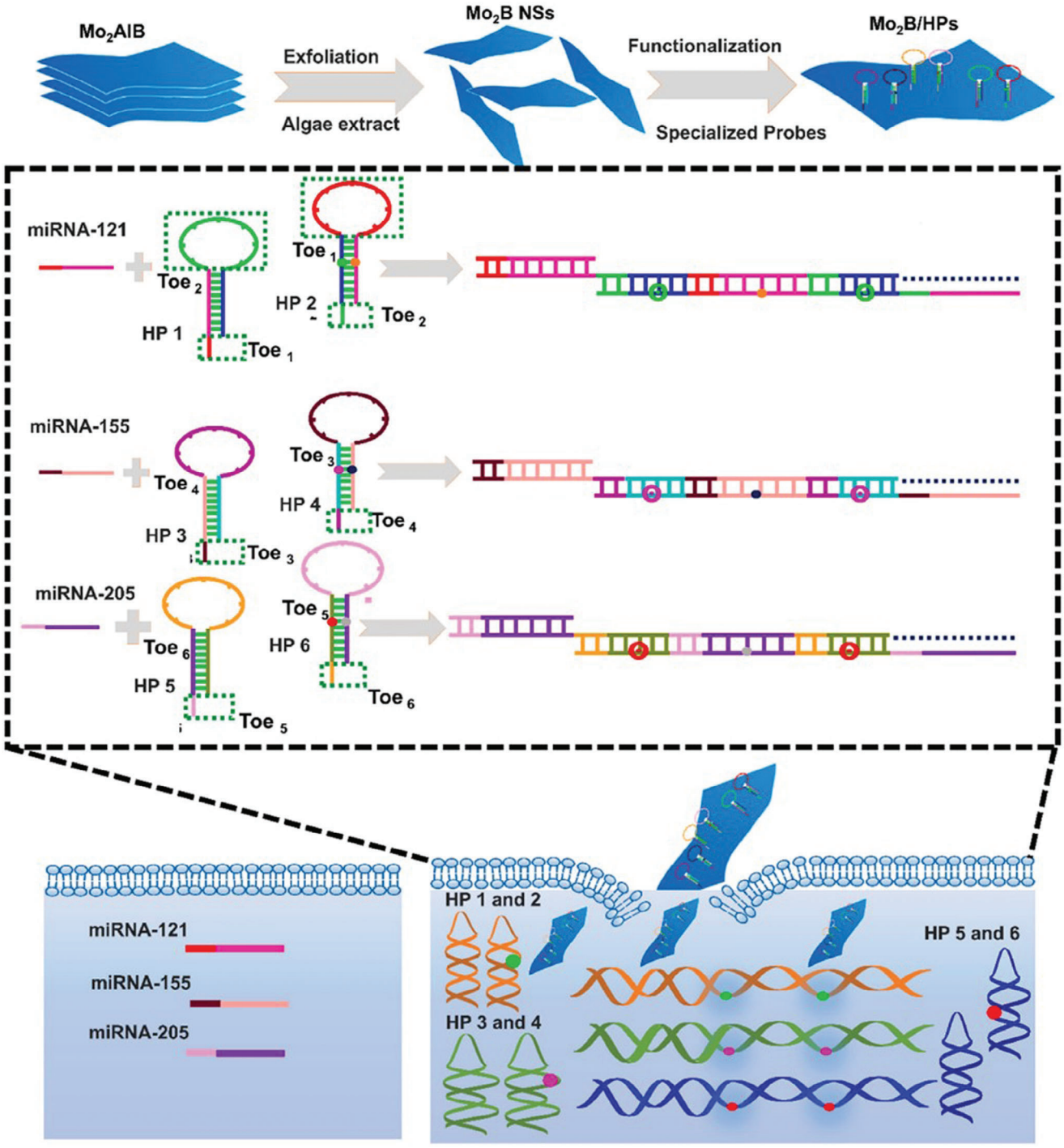

Figure 10. a) Schematic presentation of Mo_2B nanosheets-based fluorescence quenching platform for imaging multiple miRNAs in living cells using hybridization chain reaction amplification. Reprinted with permission.[99] Copyright 2022. Elsevier.

electrical systems.[102–104] MAB-phases, known for their ability to form protective tribo-films, are gaining prominence as ultra-high-temperature materials with oxidation resistance and high damage tolerance. They offer potential in high-temperature tribology, contributing to extending the lifespan of components and reducing environmental impact through the use of solid lubricants. With properties resembling both metals and ceramics, MAB-phases can be tailored for specific tribo-couples, as emphasized by Tao et al. in their use of ternary transition metal carbides, nitrides, and borides for protective surface layers in tribological applications.[105] To gain insights into potential applications of Fe_2AlB_2 and other MAB-phases, an investigation focused on its

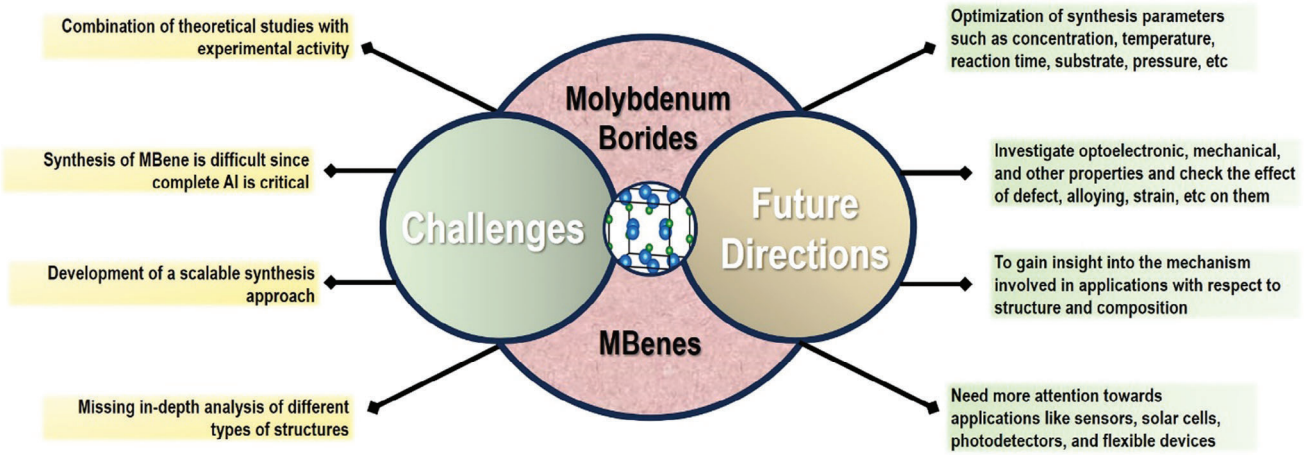

Figure 11. Schematic representation of current challenges and future perspectives for molybdenum-based borides and MBenes.

high-temperature flexural and compressive strength, along with thermal shock resistance in water from room temperature (RT) to 1000 °C. The flexural strength remained within a narrow range of 200–250 MPa across this temperature span, while the compressive strength of Fe_2AlB_2 gradually decreased from 1992 MPa at room temperature to 1482 MPa at 600 °C. A further temperature increase led to a rapid decline in compressive strength to 245 MPa at 1000 °C, despite the absence of plastic deformation.[106,107] Another study explored the friction and wear behavior of Fe_2AlB_2 against GCr^{15} steel, finding that the coefficient of friction (COF) decreased with rising sliding speed and normal force.[108] Despite variations in wear rates based on sliding speed and normal force, the wear rates ranged from 0.5 to 2.5×10^5 $mm^3(Nm)^{-1}$, attributed to the high hardness of Fe_2AlB_2. Mn_2AlB_2, identified as relatively soft for a transition metal boride, exhibited compressive strengths of 1.24 ± 0.1 GPa, indicating exceptional strength.[108] 2D MBenes are demonstrated to offer excellent lubrication properties even under high loads.[37,104] MBenes-based solid lubrication showed adequate colloidal stability with a promising reduction in friction and wear by 50% even under a load of 400 mN (contact pressure of 0.8 GPa).

5. Conclusions and Future Perspectives

Molybdenum borides have experienced a steady development both as fundamental sciences and as device applications in the past few years. This review presents the latest developments in molybdenum-based borides and MBenes. These materials are found in multiple crystallographic arrangements and therefore show unique physical and electronic properties. These materials are possible to synthesize with different strategies such as PVD, CVD, element reaction route, molten salt-assisted, and selective etching methods. In terms of applications, we mainly review the latest advancements in the fields of energy storage, catalysis, biosensors, and biomedical devices, as well as tribology and lubrication. According to studies, characteristics like large surface area, active edge sites, good conductivity, appreciable stability, and flexibility make them advantageous in achieving superior performance.

Even though significant attempts have been made to better comprehend molybdenum boride, further research is still required (**Figure 11**). Since total Al etching has not yet been achieved, the synthesis of MBene is challenging. The processes involved in etching techniques need drastic improvement. The understanding of structures and compositions of molybdenum-based boron compounds will help to prepare the structures, characteristics, and functionalities. The optimization of synthesis parameters such as concentration, temperature, reaction time, substrate, pressure, etc. requires more focus. Tailoring the properties of borides with a controlled synthesis manner can provide an opportunity to fine-tune the functionality of devices in a variety of prospective applications. The development of a scalable synthesis approach will be critical in establishing commercial uses of molybdenum boride materials. Layer and thickness-dependent studies may provide chances for device performance improvement. Also, there are several engineering approaches such as defect, strain, alloying, heterostructure fabrication, etc. that can influence the properties of materials. Though molybdenum borides have shown excellent performances in many applications, their performance is still far behind compared to other nanomaterials. The research of applications like a variety of sensors, solar cells, photodetectors, and electrocatalytic reactions is still in the early stages of research and requires more focus. There is a need for more optimization and in-depth analysis of numerous parameters involved in the application studies. Attention should be given to gain insight into the mechanism of molybdenum borides in different applications. The In situ characterization studies can be useful to gain insights into the structure. This will help to design or engineer the structure and composition of these materials as per the demand of a particular device. The study of these materials' properties is still based on theoretical hypotheses and missing experimental support for that. Thus, the combination of theoretical predictions and experimental outcomes can bring fruitful outcomes in terms of improving application performance. The progress being made in the research of molybdenum boride materials is in the primary stage, however, it appears that these materials have a bright future for variety of applications.

Acknowledgements

The authors extended their appreciation for the financial assistance provided by the SERB Core Research Grant (Grant No. CRG/2022/000897) and the Department of Science and Technology (DST/NM/NT/2019/205(G)). They also express gratitude for the support received through the Minor Research Project Grant from Jain University (JU/MRP/CNMS/29/2023). C.S.R. acknowledges backing from the National Research Foundation of Korea under the Brain Pool program, funded by the Ministry of Science and ICT, South Korea (Grant No. RS-2023-00222186). The work was further supported by the National Research Foundation of Korea (NRF) and the Commercialization Promotion Agency for R&D Outcomes (COMPA), funded by the Ministry of Science and ICT (Grant No.: RS-2023-00217581, RS-2023-00304768).

Conflict of interest

The authors declare no conflict of interest.

Keywords

2D materials, catalysis, energy storage, MBene, metal boride

Received: October 27, 2023
Revised: March 11, 2024
Published online: March 25, 2024

[1] J. Chen, Y. Lin, H. Wang, J. Li, S. Liu, J.-M. Lee, Q. Zhao, *Adv. Funct. Mater.* **2023**, *33*, 2210236.
[2] B. Zhang, J. Zhou, Z. Sun, *J. Mater. Chem. A* **2022**, *10*, 15865.
[3] H. Chen, X. Zou, *Inorg. Chem. Front.* **2020**, *7*, 2248.
[4] Z. Pu, T. Liu, G. Zhang, X. Liu, M. A. Gauthier, Z. Chen, S. Sun, *Small Methods* **2021**, *5*, 2100699.
[5] X. Wang, G. Tai, Z. Wu, T. Hu, R. Wang, *J. Mater. Chem. A* **2017**, *5*, 23471.
[6] S. Carenco, D. Portehault, C. Boissière, N. Mézailles, C. Sanchez, *Chem. Rev.* **2013**, *113*, 7981.
[7] Chinese Journal of Structural Chemistry, **2022**, *41*, 2209008.
[8] B. Albert, H. Hillebrecht, *Angew. Chem., Int. Ed.* **2009**, *48*, 8640.
[9] V. G. Nair, M. Birowska, D. Bury, M. Jakubczak, A. Rosenkranz, A. M. Jastrzębska, *Adv. Mater.* **2022**, *34*, 2108840.
[10] T. Xu, Y. Wang, Z. Xiong, Y. Wang, Y. Zhou, X. Li, *Nano-Micro Lett.* **2022**, *15*, 6.
[11] X. Zhang, A. Chen, L. Chen, Z. Zhou, *Adv. Energy Mater.* **2022**, *12*, 2003841.
[12] G. Akopov, M. T. Yeung, R. B. Kaner, *Adv. Mater.* **2017**, *29*, 1604506.
[13] W. Hua, H.-H. Sun, F. Xu, J.-G. Wang, *Rare Met.* **2020**, *39*, 335.
[14] S. K. Mellerup, S. Wang, *Chem. Soc. Rev.* **2019**, *48*, 3537.
[15] D. Rhodes, S. H. Chae, R. Ribeiro-Palau, J. Hone, *Nat. Mater.* **2019**, *18*, 541.
[16] F. Guo, Y. Wu, H. Chen, Y. Liu, L. Yang, X. Ai, X. Zou, *Energy Environ. Sci.* **2019**, *12*, 684.
[17] Y. Wang, H. Zhang, S. Jiao, K.-C. Chou, G.-H. Zhang, *J. Am. Ceram. Soc.* **2020**, *103*, 2399.
[18] X. Liu, Y. Gong, *ACS Appl. Nano Mater.* **2022**, *5*, 10183.
[19] H. Park, A. Encinas, J. P. Scheifers, Y. Zhang, B. P. T. Fokwa, *Angew. Chem., Int. Ed.* **2017**, *56*, 5575.
[20] Y. Chen, G. Yu, W. Chen, Y. Liu, G.-D. Li, P. Zhu, Q. Tao, Q. Li, J. Liu, X. Shen, H. Li, X. Huang, D. Wang, T. Asefa, X. Zou, *J. Am. Chem. Soc.* **2017**, *139*, 12370.
[21] H. Park, Y. Zhang, J. P. Scheifers, P. R. Jothi, A. Encinas, B. P. T. Fokwa, *J. Am. Chem. Soc.* **2017**, *139*, 12915.
[22] Y. Wang, C. C. Mayorga-Martinez, X. Chia, Z. Sofer, N. M. Latiff, M. Pumera, *ACS Sustainable Chem. Eng.* **2019**, *7*, 12148.
[23] R. F. Zhang, D. Legut, Z. J. Lin, Y. S. Zhao, H. K. Mao, S. Veprek, *Phys. Rev. Lett.* **2012**, *108*, 255502.
[24] A. T. Lech, C. L. Turner, R. Mohammadi, S. H. Tolbert, R. B. Kaner, *Proc. Natl. Acad. Sci. USA* **2015**, *112*, 3223.
[25] X. Qian, J. Fang, J. Xia, G. He, H. Chen, *Int. J. Hydrogen Energy* **2023**, *48*, 26084.
[26] D. V. Rybkovskiy, A. G. Kvashnin, Y. A. Kvashnina, A. R. Oganov, *J. Phys. Chem. Lett.* **2020**, *11*, 2393.
[27] J. Jin, U. Schwingenschlögl, *npj 2D Mater. Appl.* **2022**, *6*, 49.
[28] C. Avcıoğlu, S. Avcıoğlu, *Materials* **2023**, *16*, 6496.
[29] Y. Cheng, J. Mo, Y. Li, Y. Zhang, Y. Song, *Phys. Chem. Chem. Phys.* **2021**, *23*, 6613.
[30] Q. Tao, X. Zhao, Y. Chen, J. Li, Q. Li, Y. Ma, J. Li, T. Cui, P. Zhu, X. Wang, *RSC Adv.* **2013**, *3*, 18317.
[31] Z. Guo, J. Zhou, Z. Sun, *J. Mater. Chem. A* **2017**, *5*, 23530.
[32] Z. Wang, S. W. Fan, H. G. Piao, Z. S. Lu, *Appl. Surf. Sci.* **2021**, *538*, 148026.
[33] L. Yan, T. Bo, P.-F. Liu, B.-T. Wang, Y.-G. Xiao, M.-H. Tang, *J. Mater. Chem. C.* **2019**, *7*, 2589.
[34] Z. Meng, Direct synthesis of magnetic bimetallic alloy nanoparticles from organometallic precursors and their applications, **2016**.
[35] H. E. Çamurlu, *J. Alloys Compd.* **2011**, *509*, 5431.
[36] C. L. Yeh, W. S. Hsu, *J. Alloys Compd.* **2008**, *457*, 191.
[37] Q. Tao, Y. Chen, M. Lian, C. Xu, L. Li, X. Feng, X. Wang, T. Cui, W. Zheng, P. Zhu, *Chem. Mater.* **2019**, *31*, 200.
[38] P. R. Jothi, K. Yubuta, B. P. T. Fokwa, *Adv. Mater.* **2018**, *30*, 1704181.
[39] D. H. Nguyen, M. C. Ngo, Y. Tokoi, T.-M.-D. Do, T. Nakayama, H. Suematsu, K. Niihara, *J. Am. Ceram. Soc.* **2021**, *104*, 4351.
[40] F. Qi, Y. Chen, B. Zheng, J. Zhou, X. Wang, P. Li, W. Zhang, *Mater. Lett.* **2016**, *184*, 324.
[41] L. Tao, L. Han, Q. Yue, B. Yao, Y. Yang, N. Huo, *R. Soc. Open Sci.* **2021**, *8*, 210554.
[42] R. Sahu, D. Bogdanovski, J.-O. Achenbach, S. Zhang, M. Hans, D. Primetzhofer, J. M. Schneider, C. Scheu, *Nanoscale* **2021**, *13*, 18077.
[43] R. Sahu, D. Bogdanovski, J.-O. Achenbach, J. M. Schneider, C. Scheu, *Nanoscale* **2022**, *14*, 2578.
[44] M. Ozkan, K. A. M. Quiros, J. M. Watkins, T. M. Nelson, N. D. Singh, M. Chowdhury, T. Namboodiri, K. R. Talluri, E. Yuan, *Chem* **2024**, *10*, 443.
[45] D. Wu, X. Han, C. Wu, Y. Song, J. Li, Y. Wan, X. Wu, X. Tian, *J. Phys. Chem. Lett.* **2024**, *15*, 1070.
[46] W. Xiong, X. Feng, Y. Xiao, T. Huang, X. Li, Z. Huang, S. Ye, Y. Li, X. Ren, X. Wang, X. Ouyang, Q. Zhang, J. Liu, *Chem. Eng. J.* **2022**, *446*, 137466.
[47] Z. Cai, B. Liu, X. Zou, H.-M. Cheng, *Chem. Rev.* **2018**, *118*, 6091.
[48] C. Tsakonas, M. Dimitropoulos, A. C. Manikas, C. Galiotis, *Nanoscale* **2021**, *13*, 3346.
[49] J. Si, J. Yu, H. Lan, L. Niu, J. Luo, Y. Yu, L. Li, Y. Ding, M. Zeng, L. Fu, *J. Am. Chem. Soc.* **2023**, *145*, 3994.
[50] G. Gouget, D. P. Debecker, A. Kim, G. Olivieri, J.-J. Gallet, F. Bournel, C. Thomas, O. Ersen, S. Moldovan, C. Sanchez, S. Carenco, D. Portehault, *Inorg. Chem.* **2017**, *56*, 9225.
[51] D. Portehault, S. Devi, P. Beaunier, C. Gervais, C. Giordano, C. Sanchez, M. Antonietti, *Angew. Chem., Int. Ed.* **2011**, *50*, 3262.
[52] X. Liu, Y. Gong, *Inorg. Chem.* **2021**, *60*, 18075.
[53] K. Kim, C. Chen, D. Nishio-Hamane, M. Okubo, A. Yamada, *Chem. Commun.* **2019**, *55*, 9295.
[54] L. T. Alameda, P. Moradifar, Z. P. Metzger, N. Alem, R. E. Schaak, *J. Am. Chem. Soc.* **2018**, *140*, 8833.

[55] S. J. Park, T. H. Nguyen, D. T. Tran, V. A. Dinh, J. H. Lee, N. H. Kim, *Energy Environ. Sci.* **2023**, *16*, 4093.
[56] J. Zhou, J. Palisaitis, J. Halim, M. Dahlqvist, Q. Tao, I. Persson, L. Hultman, P. O. Å. Persson, J. Rosen, *Science* **2021**, *373*, 801.
[57] A. Majed, M. Torkamanzadeh, C. F. Nwaokorie, K. Eisawi, C. Dun, A. Buck, J. J. Urban, M. M. Montemore, V. Presser, M. Naguib, *Small Methods* **2023**, *7*, 2300193.
[58] A. Patra, M. Shaikh, S. Ghosh, D. J. Late, C. S. Rout, *Sustainable Energy Fuels* **2022**, *6*, 2941.
[59] A. Patra, C. S. Rout, *Energy Storage* **2023**, *5*, e411.
[60] A. Sharma, S. Bisoyi, A. Patra, G. K. Pradhan, C. S. Rout, *ACS Appl.Nano Mater.* **2022**, *5*, 17526.
[61] A. Patra, P. Mane, K. Pramoda, S. Hegde, B. Chakraborty, C. S. Rout, *J. Energy Storage* **2023**, *68*, 107825.
[62] S. Radhakrishnan, A. Patra, G. Manasa, M. A. Belgami, S. M. Jeong, C. S. Rout, *Adv. Sci.* **2024**, *11*, 2305325.
[63] J. Jia, B. Li, S. Duan, Z. Cui, H. Gao, *Nanoscale* **2019**, *11*, 20307.
[64] X.-H. Zha, P. Xu, Q. Huang, S. Du, R.-Q. Zhang, *Nanoscale Adv.* **2020**, *2*, 347.
[65] G. Barik, S. Pal, *Phys. Chem. Chem. Phys.* **2023**, *25*, 17667.
[66] T. Bo, P.-F. Liu, J. Zhang, F. Wang, B.-T. Wang, *Phys. Chem. Chem. Phys.* **2019**, *21*, 5178.
[67] Y. Xiao, Y. Li, Z. Guo, C. Tang, B. Sa, N. Miao, J. Zhou, Z. Sun, *Appl. Surf. Sci.* **2021**, *566*, 150634.
[68] J. He, A. Bhargav, A. Manthiram, *Adv. Mater.* **2020**, *32*, 2004741.
[69] Z. Guo, Y. Zhao, Y. Miao, D. Wang, D. Zhang, *ACS Appl. Energy Mater.* **2022**, *5*, 11844.
[70] Y. Cheng, Z. Li, Y. Liu, J. Qiu, R. Wang, Y. Shi, X. Niu, B. Tan, *ACS Mater. Lett.* **2023**, *5*, 2473.
[71] S. Wei, X. Lai, G. M. Kale, *ACS Appl. Mater. Interfaces* **2023**, *15*, 33560.
[72] S. Vinoth, H. T. Das, M. Govindasamy, S.-F. Wang, N. S. Alkadhi, M. Ouladsmane, *J. Alloys Compd.* **2021**, *877*, 160192.
[73] E. Lee, B. P. T. Fokwa, *Acc. Chem. Res.* **2022**, *55*, 56.
[74] H. Vrubel, X. Hu, *Angew. Chem., Int. Ed.* **2012**, *51*, 12703.
[75] P. R. Jothi, Y. Zhang, J. P. Scheifers, H. Park, B. P. T. Fokwa, *Sustainable Energy Fuels* **2017**, *1*, 1928.
[76] N. S. Peighambardoust, E. Hatipoglu, U. Aydemir, *ACS Sustainable Chem. Eng.* **2022**, *10*, 15909.
[77] A. Saad, Y. Gao, K. A. Owusu, W. Liu, Y. Wu, A. Ramiere, H. Guo, P. Tsiakaras, X. Cai, *Small* **2022**, *18*, 2104303.
[78] H. Park, Y. Zhang, E. Lee, P. Shankhari, B. P. T. Fokwa, *ChemSusChem* **2019**, *12*, 3726.
[79] Z. Zhuang, Y. Li, Z. Li, F. Lv, Z. Lang, K. Zhao, L. Zhou, L. Moskaleva, S. Guo, L. Mai, *Angew. Chem.* **2018**, *130*, 505.
[80] K. J. Baumler, L. T. Alameda, R. R. Katzbaer, S. K. O'Boyle, R. W. Lord, R. E. Schaak, *J. Am. Chem. Soc.* **2023**, *145*, 1423.
[81] N. F. Rosli, M. Z. M. Nasir, N. Antonatos, Z. Sofer, A. Dash, J. Gonzalez-Julian, A. C. Fisher, R. D. Webster, M. Pumera, *ACS Appl. Nano Mater.* **2019**, *2*, 6010.
[82] L. T. Alameda, C. F. Holder, J. L. Fenton, R. E. Schaak, *Chem. Mater.* **2017**, *29*, 8953.
[83] F. Guo, Y. Wu, X. Ai, H. Chen, G.-D. Li, W. Chen, X. Zou, *Chem. Commun.* **2019**, *55*, 8627.
[84] M. D. Scanlon, X. Bian, H. Vrubel, V. Amstutz, K. Schenk, X. Hu, B. Liu, H. H. Girault, *Phys. Chem. Chem. Phys.* **2013**, *15*, 2847.
[85] P. Helmer, J. Halim, J. Zhou, R. Mohan, B. Wickman, J. Björk, J. Rosen, *Adv. Funct. Mater.* **2022**, *32*, 2109060.
[86] X. Gao, Y. Zhou, Y. Tan, B. Yang, Z. Cheng, Z. Shen, J. Jia, *Appl. Surf. Sci.* **2019**, *473*, 770.
[87] F. Dohnal, P. Lazar, *ChemPhysChem* **2023**, *24*, 202200824.
[88] S. Dutta, H. Han, M. Je, H. Choi, J. Kwon, K. Park, A. Indra, K. M. Kim, U. Paik, T. Song, *Nano Energy* **2020**, *67*, 104245.
[89] J. G. Chen, R. M. Crooks, L. C. Seefeldt, K. L. Bren, R. M. Bullock, M. Y. Darensbourg, P. L. Holland, B. Hoffman, M. J. Janik, A. K. Jones, M. G. Kanatzidis, P. King, K. M. Lancaster, S. V. Lymar, P. Pfromm, W. F. Schneider, R. R. Schrock, *Science* **2018**, *360*, eaar6611.
[90] S. L. Foster, S. I. P. Bakovic, R. D. Duda, S. Maheshwari, R. D. Milton, S. D. Minteer, M. J. Janik, J. N. Renner, L. F. Greenlee, *Nat. Catal.* **2018**, *1*, 490.
[91] B. H. R. Suryanto, H.-L. Du, D. Wang, J. Chen, A. N. Simonov, D. R. MacFarlane, *Nat. Catal.* **2019**, *2*, 290.
[92] G. Peng, J.-W. Zhao, J. Wang, E. Hoenig, S. Wu, M. Wang, M. He, L. Zhang, J.-X. Liu, C. Liu, *Appl. Catal., B* **2023**, *338*, 123020.
[93] A. Hermawan, V. N. Alviani, Wibisono, Z. W. Seh, *iScience* **2023**, *26*, 107410.
[94] X. Liu, Z. Liu, H. Deng, *J. Phys. Chem. C* **2021**, *125*, 19183.
[95] M. Li, Y. Zhang, D. Gao, Y. Li, C. Yu, Y. Fang, Y. Huang, C. Tang, Z. Guo, *ChemPhysChem* **2024**, *25*, 202300837.
[96] Y. Xiao, C. Shen, N. Hadaeghi, *J. Phys. Chem. Lett.* **2021**, *12*, 6370.
[97] X. Lu, Y. Hu, S. Cao, J. Li, C. Yang, Z. Chen, S. Wei, S. Liu, Z. Wang, *Phys. Chem. Chem. Phys.* **2023**, *25*, 18952.
[98] X. Bai, Z. Zhao, G. Lu, *J. Phys. Chem. Lett.* **2023**, *14*, 5172.
[99] S. Zada, H. Lu, W. Dai, S. Tang, S. Khan, F. Yang, Y. Qiao, P. Fu, H. Dong, X. Zhang, *Biosens. Bioelectron.* **2022**, *197*, 113815.
[100] A. Shukla, G. Sharma, S. Krishnamurty, *Appl. Surf. Sci.* **2023**, *615*, 156299.
[101] L. Lan, X. Fan, C. Zhao, J. Gao, Z. Qu, W. Song, H. Yao, M. Li, T. Qiu, *Nanoscale* **2023**, *15*, 2779.
[102] V. S. Saji, R. M. Cook, *Corrosion Protection and Control Using Nanomaterials*, Elsevier, Amsterdam, The Netherlands **2012**.
[103] Y. Liu, S. Yu, W. Wang, *Carbon* **2022**, *198*, 119.
[104] A. Rosenkranz, Y. Liu, L. Yang, L. Chen, *Appl. Nanosci.* **2020**, *10*, 3353.
[105] Q. Tao, M. Dahlqvist, J. Lu, S. Kota, R. Meshkian, J. Halim, J. Palisaitis, L. Hultman, M. W. Barsoum, P. O. Å. Persson, J. Rosen, *Nat. Commun.* **2017**, *8*, 14949.
[106] G. Song, D. Sun, X. He, X. Qi, Y. Zheng, J. Gao, H. Yin, Y. Bai, *Ceram. Int.* **2020**, *46*, 19912.
[107] Y. Bai, D. Sun, N. Li, F. Kong, X. Qi, X. He, R. Wang, Y. Zheng, *International Journal of Refractory Metals and Hard Materials* **2019**, *80*, 151.
[108] X. Tan, P. Chai, C. M. Thompson, M. Shatruk, *J. Am. Chem. Soc.* **2013**, *135*, 9553.

Chandra Sekhar Rout is a full professor at the Centre for Nano & Material Sciences (CNMS), Jain University. Before joining CNMS, He was a DST – Ramanujan Fellow at IIT Bhubaneswar, India (2013–2017). He obtained his Ph.D. from JNCASR, Bangalore (2008) under the supervision of Prof. C.N.R. Rao followed by postdoctoral research at NUS, Purdue University, and UNIST. His research is focused on applications of 2D layered materials for different devices. He has authored more than 200 research papers and 06 books. His h-index is 57 with total citations > 13 500. He was ranked top 2% of scientists by the Stanford study in 2020–2023.

Pratik V. Shinde is currently a Postdoctoral Research Scholar at the Department of Molecular Sciences and Nanosystems, Ca' Foscari University of Venice, Italy. He received his Ph.D. at the Centre for Nano and Material Sciences, Jain University, Bengaluru, India. His research interest includes the controlled designing of composites/hybrids/heterostructures with 2D materials such as Graphene, h-BN, Metal Chalcogenides, MXene, etc. The accurate characterization of their atomic structures primarily uses various analytical techniques and explores these functionalized structures for different applications like sensors, electrocatalysis, and supercapacitors.

Abhinandan Patra was born and brought up in Puri, the spiritual capital of Odisha, India where he finished his graduation in Physics honors with distinction from Stewart Science College under Utkal University, Bhubaneshwar, Odisha, India. He received his M.Sc. degree in physics from Odisha University of Technology and Research formerly known as the College of Engineering and Technology under Biju Patnaik University of Technology (BPUT), Odisha, India with a specialization in condensed matter physics in 2019. He is presently pursuing his Ph.D. degree at the Centre for Nano and Material Sciences, Jain (Deemed-to-be) University, Bangalore, India. During the tenure of his Ph.D., he was awarded a prestigious fellowship from the Ministry of Foreign Affairs and International Cooperation (MAECI) under the Italian government. Lately, he is working on the synthesis and comprehensive characterization of novel functionalized layered 2D nanomaterials and their hybrids/composites for electrochemical storage and energy conversion applications.

Sang Mun Jeong is a professor in the Department of Chemical Engineering at Chungbuk National University, South Korea, a leader of the Regional Leading Research Center (RLRC) for developing next-generation battery materials funded by the National Research Foundation of Korea and a director of Korea Institute of Chemical Engineers. Also, he was a dean of the research affairs at Chungbuk National University (2021–2023). His research focuses on energy-related materials and processes based on chemical and electrochemical engineering to develop efficient, clean, and renewable future energy.

